Ultradipole photons in low-energy heavy-ion reactions

K. Nakayama and G. F. Bertsch
Cyclotron Laboratory, Michigan State University, East Lansing, Michigan 48824
(Received 11 June 1987)

We examine the theoretical mechanisms for producing high-energy photons in the reaction $\alpha + {}^{154}$Sm and ^{3}He + ^{148}Sm at low bombarding energies. We find that neither potential field nor nucleon-nucleon collisions can account for the measured high-energy tail, leaving the source of these photons a mystery. Further experiments are suggested to help determine the origin of the photons.

Recent measurements of high energy photons produced in heavy ion collisions[1-6] have aroused considerable interest and discussion about the production mechanisms of these photons.[7-14]

The theory of nuclear dynamics is usually based on the nuclear Hamiltonian separated into a part describing single-particle motion in a mean field potential and the remaining part treated as a residual interaction. The collisional bremsstrahlung mechanism which is due to the residual part of the Hamiltonian has been investigated by several authors[8,10-12] and it seems to provide a most important source of photon production at intermediate bombarding energies. In particular, using infinite nuclear matter approximation and considering only the first chance collisions we found in a earlier work[10] the high energy photon cross section to be of the same order of magnitude of the observed yields. The first chance collision assumption has been checked by Bauer *et al.*[12] within a model (Boltzmann-Uehling-Uhlenbeck) that contains the nucleon-nucleon collisional history of the system. In contrast, Nifenecker and Bondorf[7] and also quite recently Neuhauser and Koonin[13] assumed a statistical process for the production of energetic photons. Using a fireball model combined with an elementary nucleon-nucleon bremsstrahlung cross section those authors found a good agreement with the observed photon cross section at intermediate bombarding energies. In the calculation by Nifenecker and Bondorf[7] 15–30 collisions per participating nucleon are required in order to explain the observed yields.

The role of the potential field mechanism for photon productions in energetic heavy ion collisions has been studied in Refs. 9 and 10. Bauer *et al.*[9] using the time dependent Hartree-Fock theory have obtained photon cross section which is an order of magnitude smaller than the data for ^{12}C induced reactions at 84 MeV/nucleon bombarding energy. The semi-infinite nuclear matter approximation calculation of Ref. 10 also shows that the potential field mechanism yields a photon cross section negligible compared to the collisional mechanism at intermediate bombarding energies. However, at low incident energies one expects the potential field mechanism to dominate over the collisional one. Furthermore, the phase space available for the emission of energetic photons near their maximum energy is much smaller in the case of collisional mechanisms than in the potential field mechanism. Therefore, in the present work we investigated the contribution of the potential field mechanism in the production of high energy photons by comparing our theoretical results with the experimental data for α and ^{3}He induced reactions at 27 MeV incident energy.[6]

To evaluate the photon cross section from the potential field we apply the one-dimensional potential formula derived in Ref. 10 for the probability of photon emission per unit solid angle and unit photon energy,

$$\frac{d^2P}{d\omega\, d\Omega} = Z_{\rm p}^2 \frac{\alpha\omega}{(2\pi)^2}\frac{M_{\rm p}}{p_i p_f'} \times \sum_{\epsilon} \left| \hat{\epsilon}\cdot \int dx\, e^{ik_x x}\psi_i^*(x)\frac{\mathbf{p}}{M_{\rm p}}\psi_f(x)\right|^2 . \tag{1}$$

Here, $M_{\rm p}$ and $Z_{\rm p}$ denote the mass and number of protons of the projectile and k_x stands for the x component of the momentum $\mathbf{k}$ of the photon with energy ω. $\alpha = \frac{1}{137}$ is the fine structure constant. p_i and p_f' are defined in Eq. (3). The initial and final Wood-Saxon wave functions, ψ_i and ψ_f, with the proper normalization, have the asymptotic behaviors

$$\psi_i = \begin{cases} e^{ip_i x} + r_i e^{-ip_i x}, & x \ll 0 \\ t_i e^{ip_i' x}, & x \gg 0 \end{cases} \tag{2a}$$

and

$$\psi_f = \begin{cases} e^{\pm ip_f' x}, & x \gg 0 \\ \frac{1}{t_p} e^{ip_f x} + \frac{r_f}{t_f} e^{-ip_f x}, & x \ll 0 \end{cases} \tag{2b}$$

with the reflection and transmission amplitudes, r_β and t_β, satisfying $r_\beta^2 + (p_\beta/p_\beta')t_\beta^2 = 1$ ($\beta = i,f$). p_i and p_i' are the momenta of the projectile before and after crossing the potential well. The relation to the incident energy is

$$E_i = \frac{p_i^2}{2M_{\rm p}} = \frac{p_i'^2}{2M_{\rm p}} + V_0 . \tag{3a}$$

The momenta p_f and p_f' in the final state are given by

$$\frac{p_f^2}{2M_p}=\frac{p_i^2}{2M_p}-\omega, \quad \frac{p_f'^2}{2M_p}=\frac{p_i'^2}{2M_p}-\omega \ . \tag{3b}$$

The Wood-Saxon potential is of the form

$$V(x)=\frac{V_0}{[1+\exp(-x/a)]} \ , \tag{4}$$

with $V_0=-100$ MeV for α particles and -80 MeV for ^{3}He; $a=0.65$ fm.

In order to apply the one-dimensional formula for the photon production rate to finite nuclei, we need to average over the spherical geometry of the potential edge. Following Ref. 10 we apply Eq. (1) to the normal component of the incident momentum $\mathbf{p}_i$ to the target surface, since the acceleration is only in this direction. The normal component of $\mathbf{p}_i$ may be expressed in terms of the impact parameter b as

$$p_i^{\perp}=p_i[1-(b/R)^2]^{1/2} \ , \tag{5}$$

where, R is the radius of the target nucleus. Then, the incident energy that effectively plays a role in the photon production is that associated with $\mathbf{p}_i^{\perp}$, i.e., $E_i^{\perp}=p_i^{\perp 2}/(2M_p)$. The remaining incident energy $E_i-E_i^{\perp}$ is not available for the photon production due to the centrifugal barrier. The final momenta $p_f^{\perp}$ and $p_f^{\perp\prime}$ in this case may be determined from the total energy and momentum conservation

$$E_i=E_f+\omega \ , \tag{6a}$$

$$\mathbf{p}_i=\mathbf{p}_f+\mathbf{k} \ , \tag{6b}$$

and decomposing $\mathbf{p}_i$, $\mathbf{p}_f$, and $\mathbf{k}$ into normal and parallel components. This yields

$$\frac{p_f^{\perp 2}}{2M_p}=\frac{p_i^{\perp 2}}{2M_p}-\omega+\frac{\mathbf{p}_i^{\parallel}\cdot\mathbf{k}^{\parallel}}{M_p}-\frac{k^2}{2M_p} \ , \tag{7}$$

where, $\mathbf{p}_i^{\parallel}$ ($\mathbf{k}^{\parallel}$) denotes the parallel component of $\mathbf{p}_i$ ($\mathbf{k}$) to the target surface. The above relation differs from that of Eq. (3) by two small additional terms. Note that the parallel component $\mathbf{p}_i^{\parallel}$ will remain unchanged before and after crossing the potential well. The only change is in the normal direction to the target surface.

The Pauli principle prevents capture to states more bound than the separation energy. Consequently, this imposes a limit on the maximum photon energy. For a given incident energy $E_i=p_i^2/(2M_p)$, the maximum photon energy is

$$\omega_{\max}=\frac{p_i^{\perp 2}}{2M_p}+S \tag{8}$$

where, S denotes the separation energy.

Equations (5), (7), and (8) allow us to compute the differential probability rate for a given impact parameter b. The differential cross section is then obtained by integrating over the impact parameter and azimuthal angle

$$\frac{d^2\sigma}{d\omega\, d\Omega}=\int_0^R b\, db \int_0^{2\pi} d\phi \frac{d^2P}{d\omega\, d\Omega}\left[E=\frac{p_i^{\perp 2}}{2M_p}\right] \times\left[1-\frac{A_p}{Z_p}\frac{Z_t}{A_t}F(k)\right]^2 , \tag{9}$$

where the last factor has been introduced in order to account for the contribution due to the target current. In this factor A_t and Z_t stand for the total number of nucleons and protons in the target nucleus and $F(k)$ is the form factor of the target for photons of momentum $\mathbf{k}$ normalized to $F(0)=1$.

In order to understand the role of the finite geometry of nuclei, we show in Fig. 1(a) the integrand under the impact parameter integration in Eq. (9), i.e., the proba-

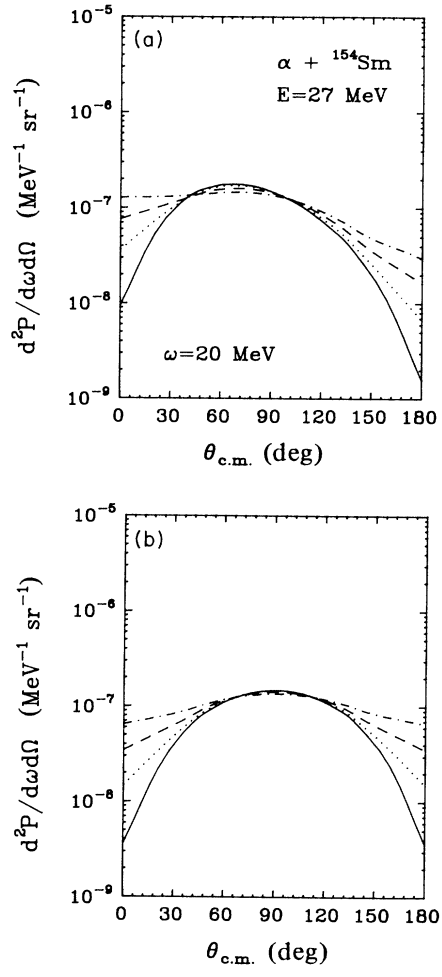

FIG. 1. (a) Photon emission rate as a function of photon emission angle in the center-of-mass frame for $\alpha+^{154}$Sm with the incident α-particle energy of 27 MeV. The photon energy was fixed to be $\omega=20$ MeV. The solid line corresponds to the impact parameter $b=1.30$ fm; the dotted line to $b=2.0$ fm; the dashed line is for $b=3.0$ fm, while the dashed-dotted line corresponds to $b=4.0$ fm. (b) Same as in (a) for the emission rate given by Eq. (10) and normalized at 90° to the corresponding curves of (a).

bility rate integrated over the azimuthal angle as a function of the impact parameter and at a fixed photon energy for the system $\alpha+{}^{154}$Sm. As one sees, the differential probability becomes more isotropic as the impact parameter increases. This can be easily understood if we remember that photons are dominantly emitted in the direction perpendicular to the velocity of the particle. As the impact parameter increases the velocity in the normal direction to the target surface becomes more and more perpendicular to the direction of the incident beam, which means that the probability rate increases at forward and backward angles as the impact parameter increases. It is interesting to compare the results of Fig. 1(a) with that obtained in Ref. 10 by observing that the probability rate is roughly independent on the incident energy. This yields a differential probability of the form

$$\frac{d^2P}{d\omega\, d\Omega} \propto 2\pi[(1-(b/R)^2)\sin^2\theta+\tfrac{1}{2}(b/R)^2(1+\cos^2\theta)] , \tag{10}$$

which is shown in Fig. 1(b) for different values of b. We see that the results show a similar behavior as in Fig. 1(a). The asymmetry around 90° observed in the case of Fig. 1(a) is due to the fact that the probability rate contains terms which go as $1/(1-\hat{\mathbf{k}}\cdot\mathbf{v})$, where $\mathbf{v}$ is the velocity of the particle. This can easily be verified by evaluating the probability rate given by Eq. (1) in the semiclassical and long wave limits. Equation (10) gives a differential probability rate which takes the pure $\sin^2\theta$ shape as b approaches zero and the $(1+\sin^2\theta/2)$ shape for b near its maximum value R.

It is also interesting to examine the influence of the centrifugal barrier on the differential cross section. As we mentioned before, the centrifugal barrier combined with the Pauli blocking enforces a limit on the maximum photon energy which is given by Eq. (8). Inverting that relation one can extract the maximum impact parameter $b_{\max}$ for a given photon energy ω at a certain incident energy E_i. This yields

$$b_{\max}=R[1-(\omega-S)/E_i]^{1/2} . \tag{11}$$

If the photon energy is small enough then all b up to R is allowed; as the ω increases $b_{\max}$ decreases. Since the differential cross section is obtained by integrating the differential probability rate over the impact parameter weighted by b, it is clear from the results of Fig. 1 that the angular distribution becomes more and more pronounced as the photon energy increases, since the larger b contribution will be suppressed. Also the results of Fig. 1 show that the near-grazing trajectories provide important contributions to the photon yield in a potential mechanism.

Within the approximation of Eq. (10) one obtains the differential cross section proportional to

$$\frac{d^2\sigma}{d\omega\, d\Omega} \propto \pi b_{\max}^2\{[1-\tfrac{1}{2}(b_{\max}/R)^2]\sin^2\theta + \tfrac{1}{4}(b_{\max}/R)^2(1+\cos^2\theta)\} . \tag{12}$$

Therefore, for photons with energies near its maximum energy the angular distribution approaches the $\sin^2\theta$ form, while for lower energies the shape is more likely $(1+\sin^2\theta/2)$. However, the exact angular distribution may differ considerably from the simple form given by Eq. (12) as is shown in Fig. 2 for photon energy of $\omega=20$ MeV.

The contribution of the target current is also very important in determining the photon cross section. For instance, for the system $\alpha+{}^{154}$Sm, it reduces the photon yield due only to the projectile current by a factor of ~ 26. Of course, as shown in Eq. (9), this reduction depends on the particular combination of the projectile and target with different Z/A ratio. In particular, for a symmetric system (in projectile and target) the photon cross section will vanish in the potential field mechanism.

Measurements of high energy photons produced in 27 MeV α and ^{3}He induced reactions have been reported in Ref. 6. These data are characterized by the temperature $T\sim 2$ MeV. The angular distribution is also asymmetric, with an implied source velocity of $\beta\sim 0.03$ (toward the direction of the projectile) with respect to the center-of-mass (c.m) system for the high energy photons. At such an incident energy and for photon energies ω near $\omega_{\max}$ we may expect the potential mechanism to be the dominant process of photon productions. In Fig. 3 we compare our results and those data for the angle integrated photon cross section and the coefficients a_1 and a_2 of the expansion of the differential cross section in terms of Legendre polynomials, $d^2\sigma/d\omega\, d\Omega = C\Sigma a_l P_l(\theta)$, where the normalization constant C is such that $a_0=1$.

We concentrate only in the high energy tail; in the region around $\omega=10-15$ MeV we observe dipole contribution which cannot be described in the present model. For lower energies the statistical process becomes dominant; one of the indication for this is the isotropic angular distribution suggested by the extracted values of a_1 and a_2 from the experimental data. As one sees, the slope of the predicted cross section is much flatter than the experiment for both α and ^{3}He cases, showing that the potential field mechanism cannot describe the high

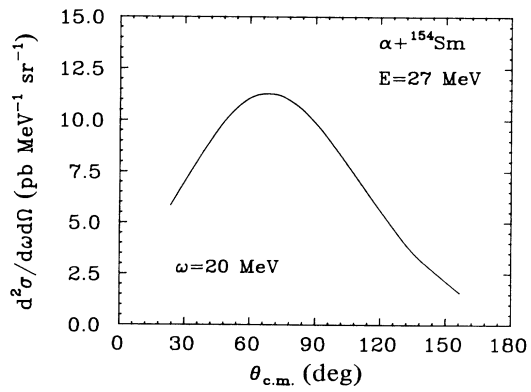

FIG. 2. Angular distribution of photons of $\omega=20$ MeV in the center-of-mass system in $\alpha+{}^{154}$Sm at 27 MeV α-particle incident energy.

tail. The reason for the larger yield obtained for ^{3}He compared to the α particle here is due to the difference in the separation energies, which are 0.65 MeV for $\alpha + ^{154}$Sm system and 9.78 MeV for ^{3}He $+ ^{148}$Sm. This implies a maximum photon energy ω_{max} of 27.0 MeV and 36.2 MeV, respectively, at $E_i = 27$ MeV incident energy (in the laboratory system). Note that in both cases we are observing photons with energies very close to the end point.

Our predicted values for a_1 and a_2 also show some discrepancies with the extracted values. There is a tendency that the predicted a_2 is somewhat larger and a_1 is smaller in magnitude than the experiment in the high energy region. However, the latter has large uncertainties. The enhancement of the predicted a_1 and a_2 as a function of ω can be easily understood from the previous discussions. Although the higher partial wave terms are not shown here, our predicted values are sizable. In particular, the magnitude of a_3 is comparable to a_1. It would be very interesting to repeat the experiment of Ref. 6 with enough angular data to determine the coefficients a_l for $l \geq 3$.

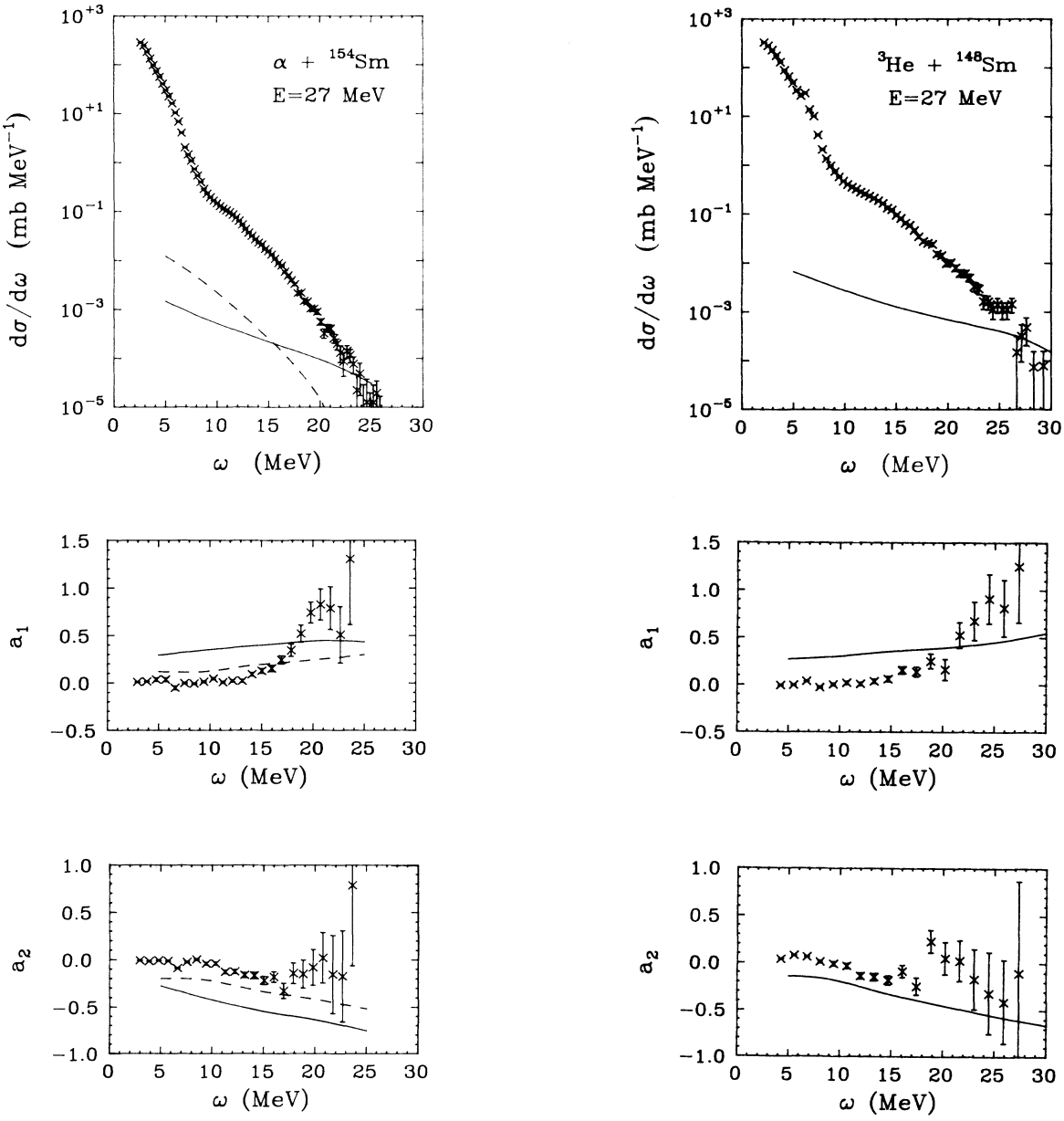

FIG. 3. Comparison between the predicted and experimental results for angle integrated cross section and the coefficients a_1 and a_2 of the expansion of the angular distribution in terms of Legendre polynomials. Normalization is such that $a_0 = 1$. The solid curves correspond to the potential field mechanism, while dashed curves to the nucleon-nucleon collisional process. The later contribution is shown only for $\alpha + ^{154}$Sm.

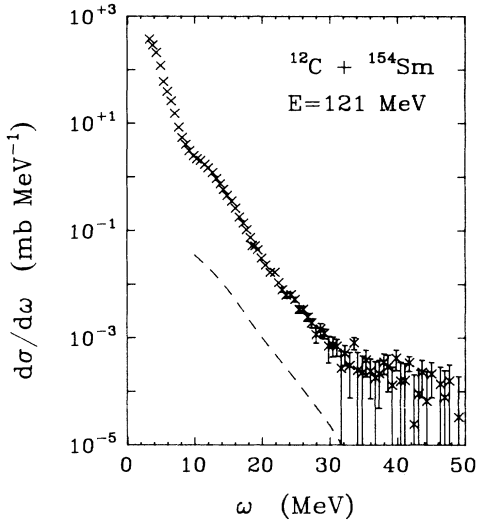

FIG. 4. Comparison between the predicted and experimental result for angle integrated cross section. The dashed curve is the prediction based on the nucleon-nucleon collisional process. The data are from Ref. 15.

At this stage one can ask about the contributions from other photon production mechanisms such as the nucleon-nucleon collisions or statistical processes. We made a rough estimate of the collisional contribution using the double Fermi sphere model of Ref. 10. Of course, one can question whether the Fermi sphere approximation adequately models the phase space distribution at this low energy and especially for nuclei as light as the α particle. However, the model does reproduce the overall features of the data at higher energy, so it is of some interest to see how it works here. The results are shown in Fig. 3 as dashed curves for $\alpha + {}^{154}$Sm. For target nucleus we took the Fermi momentum of $k_f = 1.36$ fm^{-1}, while for the α particle we adjusted the value of k_f in order to have a maximum photon energy of 27.0 MeV. This gives $k_f = 1.21$ fm^{-1} and corresponds to 70% of the nuclear matter normal density, which may be too high for α particles. As one sees, although the slope is reproduced, the calculated cross section is much smaller than the data. In Fig. 4 we also show the result for ^{12}C + ^{154}Sm at 10 MeV/nucleon bombarding energy. For the Fermi momentum of ^{12}C we assume $k_f = 1.36$ fm^{-1}. The result is similar to that of $\alpha + {}^{154}$Sm (see Fig. 3).

Also the statistical process seems to be unlikely in high energy region. The basic assumption of the statistical model for the decay of an excited system is that this system is in equilibrium before the decay process occurs. For such a system the angular distribution in the c.m. frame of the decay products is required to be symmetric around 90°. The data of Ref. 6 suggest that this is not the case for high energy photons ($a_1 \neq 0$). In addition, the cascade statistical model calculation[6] predicts a cross section which is extremely small compared to the experiment for high photon energies.

In summary, we have investigated the role of the potential field mechanism in the production of energetic photons in low energy heavy ion collisions. A comparison with the data for α and ^{3}He induced reactions at 27 MeV incident energy shows that this mechanism cannot describe the slope of the observed cross sections. Also a rough estimate of the nucleon-nucleon collisional contribution yields a cross section which is an order of magnitude smaller than the experiment. The conventional treatment of the nucleon-nucleon collisional bremsstrahlung assumes that the nucleons are on shell, ignoring the time dependence of the many-body wave function. The on shell approximation is found to fail at very low energies, and leads to consideration of partially statistical treatments as the cooperative mechanism proposed by Skyam and Knoll.[16] It may be that at very low energy one explores many-particle aspects of the process that are not important at higher beam energies. To understand the mechanism better, more experimental data are needed, for different combinations of projectile and target. It would also be helpful to study systematically the dependence of photon cross section on incident energy at low energies.

ACKNOWLEDGMENT

We would like to thank C. Gossett and K. Snover for providing us the data prior to publication. Discussion with A. Bonasera and M. Tohyama are also acknowledged. We also thank J. Behr and K. Snover for their comments. This work was supported by the National Science Foundation under Grant No. PHY85-19653.

[1] K. Beard *et al.*, Phys. Rev. C **32**, 1111 (1985).
[2] E. Grosse *et al.*, Europhys. Lett. **2**, 9 (1986).
[3] J. Stevenson *et al.*, Phys. Rev. Lett. **57**, 555 (1986).
[4] N. Alamanos *et al.*, Phys. Lett. B **173**, 392 (1986).
[5] K. Kwato Njock *et al.*, Phys. Lett. B **175**, 125 (1986).
[6] K. Snover, Annu. Rev. Nucl. Sci. **36**, 545 (1986).
[7] H. Nifenecker and J. Bondorf, Nucl. Phys. **A442**, 478 (1985).
[8] C. M. Ko, G. F. Bertsch and J. Aichelin, Phys. Rev. C **31**, 2324 (1985).
[9] W. Bauer *et al.*, Nucl. Phys. **A456**, 159 (1986).
[10] K. Nakayama and G. F. Bertsch, Phys. Rev. C **34**, 2190 (1986).
[11] W. Cassing *et al.*, Phys. Lett. B **181**, 217 (1986).
[12] W. Bauer *et al.*, Phys. Rev. C **34**, 2127 (1986).
[13] D. Neuhauser and S. E. Koonin, Nucl. Phys. **A462**, 163 (1987).
[14] B. A. Remington, M. Blann, and G. F. Bertsch, Phys. Rev. Lett. **57**, 2909 (1986); Phys. Rev. C **35**, 1720 (1987).
[15] C. Gossett and K. Snover, private communication.
[16] R. Shyam and J. Knoll, Nucl. Phys. **A426**, 606 (1984).